ACS Macro Letters

Letter

pubs.acs.org/macroletters

Origami with ABC Triblock Terpolymers Based on Glycopolymers: Creation of Virus-Like Morphologies

Aydan Dag,[†,‡] Jiacheng Zhao,[†] and Martina H. Stenzel*[,†]

[†]Centre for Advanced Macromolecular Design, School of Chemistry and School of Chemical Engineering, The University of New South Wales, Sydney, NSW 2052, Australia

[‡]Department of Pharmaceutical Chemistry, Faculty of Pharmacy, Bezmialem Vakif University, 34093 Fatih, Istanbul, Turkey

Supporting Information

ABSTRACT: Morphologies, that resemble viruses, were created using a single ABC triblock terpolymer poly(2-acryloylethyl-α-D-mannopyranoside)-*b*-poly(*n*-butyl acrylate)-*b*-poly(4-vinylpyridine) (PAcManA$_{70}$-*b*-PBA$_{369}$-*b*-PVP$_{370}$). Morphologies ranging from flower-like micelles, cylindrical micelles, raspberry-like morphologies to nanocaterpillars were obtained by adjusting the pH value during the self-assembly process. The resulting nanoparticles had an abundance of mannose on the surface, which were recognized by the mannose receptors of RAW264.7, a macrophage cell line that can be used as a model for virus entry.

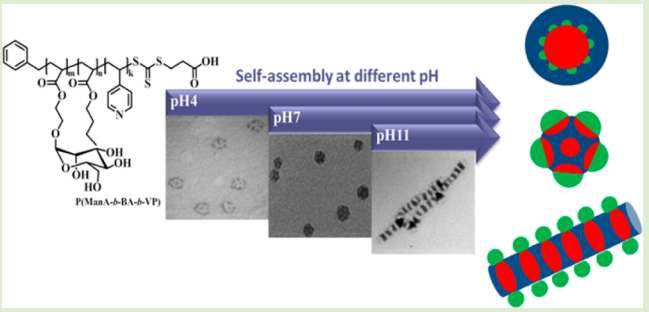

Material scientists have long turned to nature for inspiration. Many self-assembled systems such as cells are the result of millions of years of evolution and have been optimized over the course. Viruses for example are excellent survivors. Their size and shape as well as their surface chemistry allow them to invade the host without being detected, while the arrangements of their bioactive groups on the surface facilitate the entry into the host's cells. Closer inspection of the surface structure reveals the careful arrangement of glycoproteins that are essential for the binding of the virus with the target cell.[1] For example, the interaction between viruses such as HIV-1 virus and mannose receptors, which are located on dendritic cells and macrophages has been the center of attention for many years.[2,3]

The structure of viruses can be simulated by the use of self-assembled block copolymers based on mannose-derived glycopolymers. Most commonly, micelles are obtained, but also, the formation of cylindrical micelles and vesicles is possible.[4,5] Self-assembly of glycosylated block copolymers could indeed result in the formation of micelles, cylindrical micelles, and vesicles.[6−8] However, the palette of thermodynamically stable structures is rather limited although the collection can be extended by kinetically trapped aggregates. Furthermore, the surface is usually fully covered with glycopolymers in these types of aggregates, while viruses usually have a compartmentalized surface structure where the glycoproteins are placed at precise distances from each other. The use of ABC triblock terpolymers can in contrast lead to a large diversity of self-assembled structures coined multicompartment micelles (MCM).[9] The interest in these structures emerged in the late 90s when Eisenberg and co-workers created self-assembled aggregates using triblock terpolymers.[10] The seemingly endless possibilities with ABC triblock terpolymer were quickly recognized by several research groups.[9,11−13] Raspberry structures are the most common morphologies, but, as Müller and co-workers have pointed out, these assemblies are often structurally diverse, with the patch number ranging from 5−10 compartments per aggregate. Detailed investigation into the formation process led to the establishment of a guide that allows avoiding kinetically trapped morphologies to reach homogeneous multicompartment micelles.[14−17]

A range of triblock copolymers have been studied, mostly with the creation of new morphologies in mind. Looking at the structures, the resemblance to viruses is evident. Patchy raspberry-like morphologies are reminiscent of viruses with their antennae-like arrangement of glycoproteins. Bamboo-like spherical nanoparticles take on common virus-shapes with the typically elongated morphology. Stimuli-responsive polymer such as poly(2-vinylpyridine), PVP, which is a frequently used building block in the synthesis of triblock terpolymers,[18] have the advantage that they can bind to metal ions and negatively charged polymers, but their relative volume fraction can also be adjusted by different degrees of protonation. Experimental studies,[19] which were complemented by computer simulations,[20] show the transition of a water-soluble polymer in acidic media to an in water-insoluble polymer at neutral and alkaline pH.

In this communication, we venture away from traditional ABC triblock terpolymer systems and apply the existing

Received: March 5, 2015
Accepted: April 29, 2015
Published: May 4, 2015

DOI: 10.1021/acsmacrolett.5b00163
ACS Macro Lett. 2015, 4, 579−583

knowledge to mannose-containing glycopolymers[21−24] (Scheme 1), which have high activity toward macrophages and therefore serve as a model of surface ligands found on viruses. Only one ABC triblock terpolymer was necessary to create different structures since the morphology could simply be influenced by adjusting the solution pH.

Scheme 1. Synthesis of Triblock Copolymer and Its Self-Assembly in Methanol Followed by Dialysis against Aqueous Solutions of Different pH Values[a]

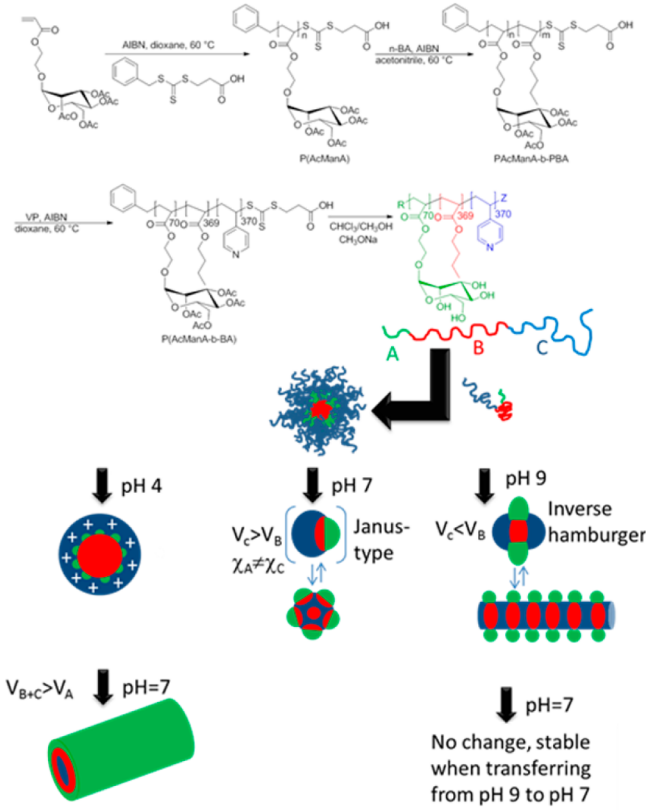

[a]V_A, V_B, and V_C = relative volume of block A, B, and C, respectively; χ_A, χ_B, and χ_C = Flory−Huggins interaction parameters.

The triblock copolymer was prepared using RAFT (reversible addition−fragmentation chain transfer) polymerization.[25] Poly(2-acryloylethyl-2′,3′,4′,6′-tetra-*O*-acetyl-α-D-mannopyranoside) macroRAFT agent was synthesized from synthesized from 2-acryloylethyl-2′,3′,4′,6′-tetra-*O*-acetyl-α-D-mannopyranoside in the presence of 3-(benzylthiocarbonothioylthio)propanoic acid and 1 mol % of fluorescein *o*-acrylate (Supporting Information (SI), Figures S1−S8). The polymer was then chain-extended with *n*-butyl acrylate at a high monomer to macroRAFT agent ratio to generate a large hydrophobic block with the intention to create large self-assembled features (SI, Figures S9 and S10). The purified block copolymer P(AcManA$_{70}$-*b*-PBA$_{369}$) was subsequently reacted with 4-vinylpyridine (VP) yielding the ABC triblock terpolymer (PAcManA$_{70}$-*b*-PBA$_{369}$-*b*-PVP$_{370}$) (SI, Figure S11), which was deactylated to generate the final block copolymer (SI, Figure S12). The polymers were characterized at each step using ^{1}H NMR and GPC analysis (SI, Figures S7, S10−S12), confirming the formation of a well-defined ABC triblock terpolymer (Table 1).

Methanol was identified as a suitable selective solvent since both PVP and PManA are soluble while PBA is not. Direct dissolution of the polymer in methanol led to the collapse of PBA resulting in the formation of a mixed glycopolymer and PVP corona. Dynamic light scattering (DLS) analysis at this point revealed a hydrodynamic diameter of 80 nm (SI, Figure S13). The methanol solution was subsequently dialyzed against aqueous solutions of different pH values, such as pH 2, 4, 7, 9, and 11. Taking the literature reported pK_a value for PVP of 5.0 into account[26] and assuming the validity of the Henderson−Hasselbalch equation in this scenario,[26] the degree of ionization was calculated to be ∼99 (pH 2), ∼90 (pH 4), ∼1 (pH 7), and ≪1% at pH 9 and 11. Depending on the degree of ionization PVP turned from a neutral, in water-insoluble polymer, to a cationic and water-soluble polymer. The degree of ionization will therefore not only determine the solubility in water and the compatibility with the water-soluble glycopolymer, but also the volume *V* of this polymer, since higher ionization will lead to repulsion.

At pH 2 or 4, the almost fully ionized PVP micelles with hydrodynamic diameters of 160 and 153 nm, respectively, were formed (Figure 1A and SI, Figures S14 and S15). Only little or no compartmentalization takes place as evidenced by the almost even distribution of PVP (black as a result of OsO_4 staining). Since V_{PVP} is larger than V_{PMan}, it can safely be assumed that most of the glycopolymer is buried under a layer of cationic charged PVP polymer. Zetapotential measurements reveal indeed a high positive surface charge of +42 mV, which is indicative of coverage of the surface of the nanoparticles with protonated PVP.

Dialysis of the polymer solution from methanol against an aqueous solution of pH 7 leads to almost complete deprotonation of the PVP polymer although it is estimated that a small percentage (around 1%) of cationic charges remains. The deprotonated polymer is insoluble in water resulting in the collapse of PVP. A small percentage of

Table 1. Molecular Characteristics of the Triblock Copolymers and Their Precursors

polymer	[M]/[FlsAcr]/[RAFT]/[I]	time (h)	conv[a] (%)	$M_{n,th}$ (kDa)	$M_{n,NMR}$ (kDa)	SEC[f] M_n(kDa)	SEC[f] $Đ$
P(AcManA$_{70}$)	100/1/1/0.1	7	70	25[b]	31[e]	15	1.27
PAcManA$_{70}$-*b*-PBA$_{369}$	900//1/0.2	2.16	41	69[c]	78[e]	32	1.26
PAcManA$_{70}$-*b*-PBA$_{369}$-*b*-PVP$_{370}$	420//1/0.4	20	88	108[d]	117[e]	61	1.28
PManA$_{70}$-*b*-PBA$_{369}$-*b*-PVP$_{370}$)		3	96	106	106	85	1.13

[a]Obtained from ^{1}H NMR analysis. [b]Calculated from according to eq = $[M]_0/[RAFT]$ × conv.% (isolated yield) × MW of AcManA + MW of RAFT agent. [c]Calculated from according to eq = $[M]_0/[RAFT]$ × conv.% (isolated yield) × MW of *n*BA + MW of Macro RAFT agent. [d]Calculated from according to eq = $[M]_0/[RAFT]$ × conv.% (isolated yield) × MW of VP + MW of Macro RAFT agent. [e]Calculated according to eq = $[M]_0/[RAFT]$ × conv.% (from NMR) × MW of *n*BA + MW of Macro RAFT agents. [f]Determined from DMAc GPC (relative to PS standards).

DOI: 10.1021/acsmacrolett.5b00163
ACS Macro Lett. 2015, 4, 579−583

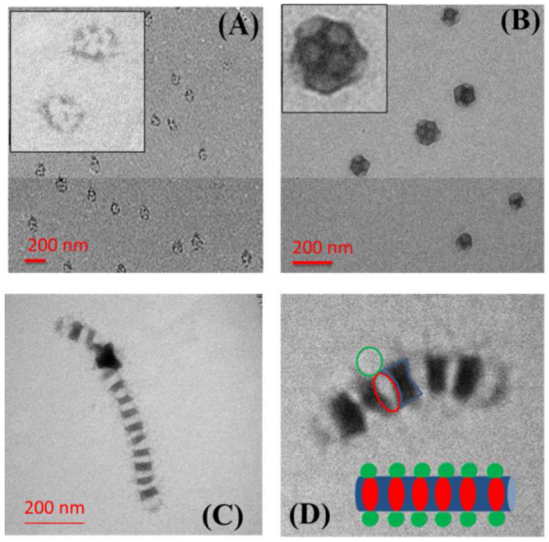

Figure 1. Representative TEM images of $PManA_{70}$-*b*-PBA_{369}-*b*-PVP_{370} glyco-nanoparticles obtained at various pH values (A: pH 4; B: pH 7; C, D: pH 9). Staining was obtained with UAc and OsO_4 (PVP black, PBA gray, PManA invisible).

remaining cationic charges may allow some swelling of the polymer and, based on TEM evidence (Figure 1B and SI, Figure S16), these remaining charges may be sufficient to have a relative volume of V_{PVP} bigger than V_{PBA}. At the same time, PVP became incompatible with the glycopolymer, which led to the formation of compartmentalized structures that have diameters of around 120 nm (TEM) and a hydrodynamic diameter of 123 nm. The intermediate formation of Janus-type structures have been suggested,[14] followed by the aggregation of several units into raspberry-like structures, here "football" MCMs, which are indicated by around eight light PBA patches surrounded by a dark (OsO_4 stained) PVP matrix. The glycopolymer is then concentrated only to specific areas, although direct visualization of the glycopolymer was not possible since a suitable staining agent could not be found. The obtained structure has a certain resemblance to adenoviruses, which typically have sizes of approximately 100 nm bearing similar surface structures, although they have more patches on the surface and therefore smaller features.

At pH 9, which coincided with almost complete deprotonation of PVP, the PVP chain collapsed further, minimizing its space requirement. With V_{PVP} now being equivalent to V_{PBA}, the nanosegregated polymer structures lead to "hamburgers", which are the result of two Janus-type structures, depicted in Scheme 1, being glued together via the PBA block while the glycopolymer block A was pushed aside to form the shell. Addition of several units of these hamburgers resulted in the formation of rod-like structures with segmented morphologies, reminiscent of caterpillars (Figure 1C and SI, Figure S17). Although the glycopolymer PManA is invisible under TEM, the shadow of this block can be identified at higher resolution (Figure 1D). The length of these caterpillars was approximately 400−1000 nm according to TEM, while DLS revealed a hydrodynamic diameter of 170 nm (SI, Figure S14). The obtained structures resemble filaviruses. The Marburg virus is around 790 nm long, while the Ebola virus has a length of 970 nm. The diameters of 80 nm is, however, smaller than the structures obtained here. Both viruses have glycoproteins placed in regular distances from each other.

The process was also applied by dialyzing against aqueous solutions of pH 11. Dialysis against pH 11 caused the collapse of the caterpillar structures and led to heavily aggregated morphologies. DLS analysis showed now the presences of large size tail (SI, Figure S14). The observed structures may suggest complete dehydration of PVP (SI, Figure S18).

These morphologies discussed above were prepared at pH values ranging from 2 to 12. However, solutions of pH values that deviate considerably from pH 7 are not suitable for investigations into the bioactivity since it will cause adverse effects in the cells. Therefore, the glyco-nanoparticles solutions at pH 4 and 9 were dialyzed against water at pH 7 using dialysis. Interestingly, the caterpillar morphologies prepared at pH 9 were stable for several hours. After 18 h, some disassociation can be identified. However, the vast majority is still in the rod-like form indicating strong intermolecular forces between the hydrophobic polymers. The absence of significant changes is not surprising considering that PVP is insoluble at pH 7 and pH 9. More dramatic effects are in contrast obtained when the solution with flower-like structures, prepared at pH 4, is dialyzed against water of neutral pH. In this scenario PVP will be deprotonated again resulting in a small water-soluble glycopolymer block, while PBA and PVP are both insoluble. Instead of transforming into the football morphology, the ABC terpolymers rearrange into cylindrical micelles without any apparent patterning at the surface suggesting the arrangement of the polymer, as depicted in Scheme 1. The transition was found to be very fast: A few minutes after the influx of the neutral aqueous solution into the nanoparticle solution at pH 4, the solution in the dialysis bag turned cloudy, which coincides with the formation of larger particles, as evidenced by DLS (Figure 2). To gather more information about this molecular

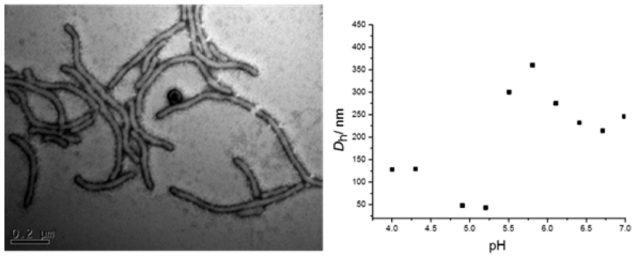

Figure 2. Transition of the flower-like morphologies obtained from pH 4 into cylindrical micelles at pH 7; left, TEM after switching of the solution from pH 4 to pH 7; right, hydrodynamic diameter D_h after adjusting the solution at pH 4 to various pH values.

rearrangement, the pH value of the solution was changed gradually. With increasing pH value, the PVP corona becomes more and more insoluble in water. The corona starts collapsing resulting in nanoparticles of smaller hydrodynamic diameter. Although one would expect that further deprotonation would result in precipitation, the solution remained stable throughout the process. At around pH 5.5, the hydrodynamic diameter increased suddenly, which probably coincides with the transition to cylindrical micelles (Figure 2). It is most likely that the low T_g of PBA facilitated this process, which required significant chain rearrangement. In future work, this rearrangement process can be prevented by cross-linking the structures.[27]

Three stable solutions at pH 7 (cylindrical micelles, raspberry-like morphologies, and nanocaterpillars) have now been prepared. The nanoparticles did not show any signs of

DOI: 10.1021/acsmacrolett.5b00163
ACS Macro Lett. 2015, 4, 579−583

change within a few days although two morphologies are only kinetically trapped while only one can be thermodynamically stable. It is not possible at the moment to identify the morphology that is thermodynamically stable at pH 7.

These solutions at pH 7 can now be safely employed for further biological investigation while the morphology are resistant to aggregate changes. Stabilization by cross-linking is therefore not necessary at this point. The polymer was labeled with fluorescein-*o*-acrylate to be able to monitor the cellular uptake. The presence of glycopolymer can quickly be confirmed using a turbidity assay based on ConA, which is specific to mannose.[24] All three aggregates, cylindrical micelles, raspberry-like morphologies, and nanocaterpillar, showed fast and efficient binding with ConA (SI, Figure S17). Although some conclusions could be drawn in regards to the rate of binding, the turbidity assay is rather a qualitative assay confirming the presence of bioactive groups than a quantitative one.[22,28]

Subsequently, the interaction of these nanoparticles with macrophages was explored. The macrophage cell line RAW264.7 carries a high density of mannose receptors and is therefore considered suitable for this study.[29] The cytotoxic effect of P($ManA_{70}$-*b*-BA_{369}-*b*-VP_{370}) glyco-nanoparticles in the raspberry-like morphology on the RAW264.7 cells was determined by a standard sulforhodamine B colorimetric assay (SRB assay). The results of the SRB-assay, shown in SI, Figure S18, reveal an IC_{50} of 133.3 μg/mL. The modest toxicity can be assigned to the presence of PVP, which has a small proportion of potentially cytotoxic cationic charges. Since the various morphologies were prepared with the same polymer, it is expected that this results does not vary noticeably from nanoparticle to nanoparticle. There may be some small variations in toxicity caused by the differences in cellular uptake.

The specific cellular uptake of mannosylated polymers and nanoparticles is well-known.[30−32] Macrophages were found to have a higher affinity to mannose-coated nanoparticles than to PEG-coated particles.[33,34] The uptake of the nanoparticles was monitored by flow cytometry and confocal fluorescent microscopy. The fluorescence intensity was additionally quantified to ensure that changes to the fluorescence intensity during the nanoparticle preparation were taken into account. The actual fluorescence intensity of each nanoparticle was used to adjust the flow cytometry values. All the experiments were performed at a concentration of 100 μg/mL, a concentration that can be considered nontoxic according to the SRB assay (nontoxic is considered >80% cell viability). After 24 h, the green fluorescent nanoparticles are clearly visible within the cytosol (Figure 3I). Overlay of the lysosome (stained in red with lysotracker) and the nanoparticles show the colocalization indicative of endocytosis. Initial inspection of the fluorescence of the three morphologies revealed a higher uptake by the worm-like structures (Figure 3II) although fluorescence microcopy can only provide an initial estimate. Flow cytometry was employed to quantify the uptake (Figure 3III and SI, Figure S20). It seems that RAW264.7 cell have a slightly lower affinity to spherical nanoparticles. This is in agreement with other results that showed the better uptake of worm-like aggregates compared to spherical micelles.[35,36] One aspect to consider is that the number of particles is higher in the raspberry-like micelle solutions since less polymer is required to build up one particle. More details on this matter will be revealed in future concentration-dependent uptake studies.

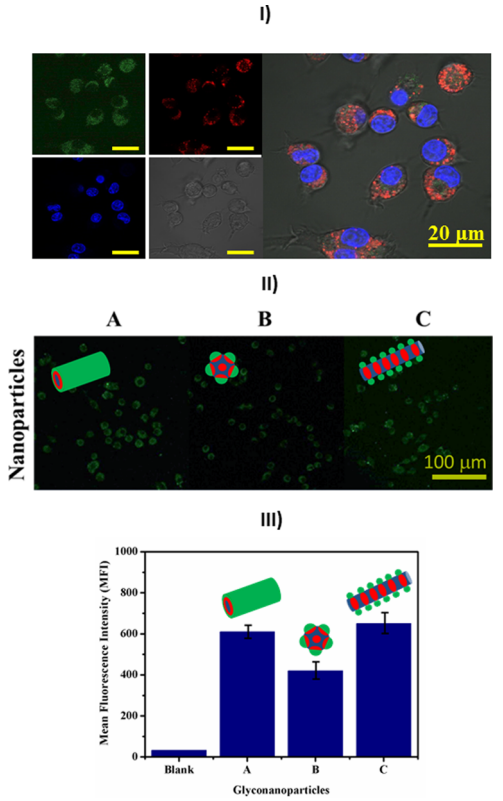

Figure 3. (I) Internalization of glyco-nanoparticles (raspberry-like nanoparticles) at pH 7 by RAW264.7 cells measured by confocal fluorescence microscopy: green, micelles; red, lysosome; blue: nuclei (scale bar: 20 μm); (II) Cellular uptake of glyco-nanoparticles by RAW264.7 cells prepared at various pH: (A) pH = 4; (B) pH = 7; (C) pH = 9 and subsequently adjusted to pH 7; (III) Flow cytometry analysis of cellular uptake of glyco-nanoparticles by RAW264.7 cells after 24 h of incubation at 37 °C (50000 cells).

In this communication we showed that the lessons learned from the self-assembly of ABC terpolymers can be applied to bioactive polymer such as glycopolymers to create morphologies that are reminiscent of the structures found in nature such as viruses. One block copolymer is sufficient to generate a range of morphologies as long as one block has stimuli-responsive features such as here pH-responsive groups. This made it possible that one block copolymer led to flower-like micelles, cylindrical micelles, raspberry-like morphologies, and nanocaterpillar, depending on the processing conditions. These morphologies were found to be bioactive and were efficiently taken up by cells. The chosen RAW264.7, which has a strong affinity to mannose, was found to have a slight preference for worm-like aggregates over spherical morphologies.

■ ASSOCIATED CONTENT

Supporting Information

Synthesis of polymers and their NMR analysis, DLS data of self-assembled structures, and TEM analysis of polymers prepared at pH 2 and 11. Turbidity assay to monitor the reaction with ConA, and cell viability data of RAW 264.7 after treating with polymer. The Supporting Information is available free of charge on the ACS Publications website at DOI: 10.1021/acsmacrolett.5b00163.

DOI: 10.1021/acsmacrolett.5b00163
ACS Macro Lett. 2015, 4, 579−583

AUTHOR INFORMATION

Corresponding Author

*E-mail: m.stenzel@unsw.edu.au.

Notes

The authors declare no competing financial interest.

ACKNOWLEDGMENTS

The authors thank the UNSW Mark Wainwright Analytical Centre for help. Funding is acknowledge from the Australian Research Council (DP DP130101625), The Scientific and Technological Research Council of Turkey (TUBITAK; Project No: 1059B191200208), and China Scholarship Council (CSC).

REFERENCES

(1) Kalia, M.; Jameel, S. *Amino Acids* **2011**, *41*, 1147−1157.
(2) Liu, K.-J. *J. Cancer Mol.* **2006**, *2*, 213−215.
(3) Turville, S. G.; Arthos, J.; Mac Donald, K.; Lynch, G.; Naif, H.; Clark, G.; Hart, D.; Cunningham, A. L. *Blood* **2001**, *98* (8), 2482−2488.
(4) Mai, Y.; Eisenberg, A. *Chem. Soc. Rev.* **2012**, *41* (18), 5969−5985.
(5) Blanazs, A.; Armes, S. P.; Ryan, A. J. *Macromol. Rapid Commun.* **2009**, *30* (4−5), 267−277.
(6) Kramer, J. R.; Rodriguez, A. R.; Choe, U.-J.; Kamei, D. T.; Deming, T. J. *Soft Matter* **2013**, *9* (12), 3389−3395.
(7) You, L.; Schlaad, H. *J. Am. Chem. Soc.* **2006**, *128* (41), 13336−13337.
(8) Ladmiral, V.; Semsarilar, M.; Canton, I.; Armes, S. P. *J. Am. Chem. Soc.* **2013**, *135* (36), 13574−13581.
(9) Moughton, A. O.; Hillmyer, M. A.; Lodge, T. P. *Macromolecules* **2011**, *45* (1), 2−19.
(10) Yu, G.-E.; Eisenberg, A. *Macromolecules* **1998**, *31* (16), 5546−5549.
(11) Bivigou-Koumba, A. M.; Gornitz, E.; Laschewsky, A.; Muller-Buschbaum, P.; Papadakis, C. M. *Colloid Polym. Sci.* **2010**, *288* (5), 499−517.
(12) Marsat, J. N.; Heydenreich, M.; Kleinpeter, E.; Berlepsch, H. V.; Bottcher, C.; Laschewsky, A. *Macromolecules* **2011**, *44* (7), 2092−2105.
(13) Skrabania, K.; von Berlepsch, H.; Bottcher, C.; Laschewsky, A. *Macromolecules* **2010**, *43* (1), 271−281.
(14) Groschel, A. H.; Schacher, F. H.; Schmalz, H.; Borisov, O. V.; Zhulina, E. B.; Walther, A.; Muller, A. H. E. *Nat. Commun.* **2012**, *3*, 710.
(15) Groschel, A. H.; Walther, A.; Lobling, T. I.; Schacher, F. H.; Schmalz, H.; Muller, A. H. E. *Nature* **2013**, *503* (7475), 247.
(16) Hanisch, A.; Groschel, A. H.; Fortsch, M.; Drechsler, M.; Jinnai, H.; Ruhland, T. M.; Schacher, F. H.; Muller, A. H. E. *ACS Nano* **2013**, *7* (5), 4030−4041.
(17) Wolf, A.; Walther, A.; Muller, A. H. E. *Macromolecules* **2011**, *44* (23), 9221−9229.
(18) Lei, L.; Gohy, J.-F.; Willet, N.; Zhang, J.-X.; Varshney, S.; Jérôme, R. *Macromolecules* **2003**, *37* (3), 1089−1094.
(19) Martin, T. J.; Procházka, K.; Munk, P.; Webber, S. E. *Macromolecules* **1996**, *29* (18), 6071−6073.
(20) Posel, Z.; Limpouchová, Z.; Šindelka, K.; Lísal, M.; Procházka, K. *Macromolecules* **2014**, *47* (7), 2503−2514.
(21) Becer, C. R. *Macromol. Rapid Commun.* **2012**, *33* (9), 742−752.
(22) Miura, Y. *Polym. J.* **2012**, *44* (7), 679−689.
(23) Kiessling, L. L.; Grim, J. C. *Chem. Soc. Rev.* **2013**, *42* (10), 4476−4491.
(24) Ting, S. R. S.; Chen, G. J.; Stenzel, M. H. *Polym. Chem.* **2010**, *1* (9), 1392−1412.
(25) Gregory, A.; Stenzel, M. H. *Prog. Polym. Sci.* **2012**, *37* (1), 38−105.
(26) Yoshida, M. *Eur. Polym. J.* **1997**, *33* (6), 943−948.
(27) Utama, R. H.; Drechsler, M.; Foerster, S.; Zetterlund, P. B.; Stenzel, M. H. *ACS Macro Lett.* **2014**, *3* (9), 935−939.
(28) Chen, Y.; Lord, M. S.; Piloni, A.; Stenzel, M. H. *Macromolecules* **2015**, *48* (2), 346−357.
(29) Morishima, S.; Morita, I.; Tokushima, T.; Kawashima, H.; Miyasaka, M.; Omura, K.; Murota, S. *J. Endocrinol.* **2003**, *176* (2), 285−92.
(30) Kim, N.; Jiang, D.; Jacobi, A.; Lennox, K. A.; Rose, S.; Behlke, M. A.; Salem, A. K. *Int. J. Pharm.* **2012**, *427* (1), 123−133.
(31) Jiang, H.-L.; Kang, M. L.; Quan, J.-S.; Kang, S. G.; Akaike, T.; Yoo, H. S.; Cho, C.-S. *Biomaterials* **2008**, *29* (12), 1931−1939.
(32) Niu, M.; Naguib, Y. W.; Aldayel, A. M.; Shi, Y.-c.; Hursting, S. D.; Hersh, M. A.; Cui, Z. *Mol. Pharmaceutics* **2014**, *11* (12), 4425−4436.
(33) Zhu, S.; Niu, M.; O'Mary, H.; Cui, Z. *Mol. Pharmaceutics* **2013**, *10* (9), 3525−3530.
(34) Yu, S. S.; Lau, C. M.; Barham, W. J.; Onishko, H. M.; Nelson, C. E.; Li, H.; Smith, C. A.; Yull, F. E.; Duvall, C. L.; Giorgio, T. D. *Mol. Pharmaceutics* **2013**, *10* (3), 975−87.
(35) Zhang, K.; Rossin, R.; Hagooly, A.; Chen, Z.; Welch, M. J.; Wooley, K. L. *J. Polym. Sci., Part A: Polym. Chem.* **2008**, *46* (22), 7578−7583.
(36) Alemdaroglu, F. E.; Alemdaroglu, N. C.; Langguth, P.; Herrmann, A. *Macromol. Rapid Commun.* **2008**, *29* (4), 326−329.

DOI: 10.1021/acsmacrolett.5b00163
ACS Macro Lett. 2015, 4, 579−583